

A novel motion monitoring system for activities of daily living

X. He¹ and A. Farajidavar^{1,*}

¹1st Integrated Medical Systems Laboratory, School of Engineering and Computing Sciences, New York Institute of Technology, Northern Blvd., Old Westbury, New York 11568.

¹2nd Integrated Medical Systems Laboratory, School of Engineering and Computing Sciences, New York Institute of Technology, Northern Blvd., Old Westbury, New York 11568.

Abstract

Capability to perform activities of daily living (ADLs) is a major factor in quality of life (QOL). While it can be difficult for the elderly, disabled, or patients with chronic diseases to deal with ADLs, they need to spend a great deal of money on healthcare and assistive technologies to keep a good QOL. The situation can be improved if a real-time ADLs monitoring and recognition system is available to provide health information to physicians, pharmacists, or caregivers to offer timely diagnosis, prescription, or emergency reaction.

We have developed a wireless wearable motion monitoring system that is suitable for monitoring ADLs involving limbs. The system consists of six Bluetooth low energy (BLE) transponders that are small and light enough to be mounted on all limbs. Each transponder, called SensorTag (by Texas Instruments), is equipped with a tri-axial accelerometer, a tri-axial magnetometer, and a tri-axial gyroscope for motion monitoring. Each SensorTag can be linked to a smartphone for long-term outdoor monitoring. A graphic user interface is created to acquire signals from BLE receivers, display the signals in real-time, process data, and store for off-line analysis.

This system was tested in three scenarios, and signals were analyzed off-line using a quaternion-based motion reconstruction algorithm. First, a SensorTag was examined against a marker-based motion capture system in a linear motion test. Second, a SensorTag was worn on a subject's wrist to monitor food-intake trajectory. Finally, six SensorTags were worn on wrist, knee, and ankle joints of left and right hands to monitor gait on a straight path. Results showed various error rates in different scenarios, however, the error rates are within an acceptable range, and more importantly the patterns of the motions are reproducible.

Keywords: inertial measurement unit, motion monitoring, activities of daily living.

Received on 30 August 2016, accepted on 24 October 2016, published on 21 March 2017

Copyright © 2017 X. He and A. Farajidavar, licensed to EAI. This is an open access article distributed under the terms of the Creative Commons Attribution licence (<http://creativecommons.org/licenses/by/3.0/>), which permits unlimited use, distribution and reproduction in any medium so long as the original work is properly cited.

doi: 10.4108/eai.21-3-2017.152392

1. Introduction

1.1. Motivation for monitoring activities of daily living

Activities of daily living (ADLs) are generally categorized in to two main categories [1]. The first type is the basic ac-

tivities of daily living (BADLs), which includes self-care tasks such as bathing, dressing, toileting, brushing teeth, eating and functional mobility. The other type is the instrumental activities of daily living (IADLs), which allows people to keep an independent lifestyle with additional services, such as cooking, driving, using telephone or computer, shopping, keeping track of finances and managing medication [2, 3]. The ability to perform ADLs is a major factor in determining one's quality of life (QOL) [4, 5, and 6]. While

*Corresponding author. Email:afarajid@nyit.edu

it can be very difficult for elderly, disabled or chronic disease patients to deal with ADLs, they also need to spend so much on healthcare and assistive technologies to keep a reasonable QOL.

The problem becomes more serious as the aging population is growing. According to the report by the Population Division (a contribution to the 2002 World Assembly on Ageing and its follow-up), the number of aging people in the world has been increasing every year since 1950 [7]. Muscle strength, balance and body function declines with aging, and the possibility of neurodegenerative diseases such as Parkinson's disease (PD) increases [8].

PD patients, for example, have typical symptoms like rest tremor, bradykinesia, hypokinesia or rigidity [9]. Most tremors happen at hands or fingers resulting in failed attempts to perform ADLs like holding forks. Apart from the difficulties in executing ADLs, the therapy relies on the PD patient's symptoms [10, 11]. Different dosage should be prescribed according to the symptom reports, which can be extracted from the motor features report in diaries. However, the report can only cover a short period of time. As a result, researchers have developed various systems to monitor these symptoms and ADLs. A summary of the state-of-the-art of the monitoring systems, which can capture the motion, is explained in the following section.

1.2. Current state-of-the-art of motion monitoring technologies and shortcomings

Various technologies have been used for human body monitoring. A summary of these technologies with their pros and cons is shown in Table 1. Human motion monitoring with markers has been used for human body and body part motion analysis since Johansson's (1973) moving light display psychological experiment [12]. Although the marker-based optical motion capture (mo-cap) systems provide very accurate motion data, they are expensive to setup and the monitoring space is limited [13]. With the development of Microelectromechanical systems (MEMS) devices, inertial sensors are used in some simple applications like video gaming consoles and smartphones for orientation computation [14]. Wii MotionPlus is a typical remote controller with more accurate motion sensing abilities, but it can be easily deceived because it only monitors the player's hand motion, and the player can sit on a couch and pretend to play tennis or golf. In other words the console does not provide whole body motion monitoring. The advantages of inertial measurement unit (IMU) sensing devices are that they are easy to setup, small to wear, and they are cheaper than the optical camera system. However, their information is not as accurate as mo-cap systems. The sensor data drifts as time progresses and there is a lack of a reference system to fix the error [15].

In IMUs, gyroscope measures the angular rate for orientation [16]. However, it drifts over time and needs the direction of gravity (accelerometer) or earth magnetic field (magnetometer) as reference for revision [17, 18, and 19]. This type of sensor that can measure magnetic, angular rate, and

Table 1. Comparison of marker-based optical motion capture (mo-cap) system, depth sensing camera or scanner and inertial sensors mo-cap system.

System type	Marker-based optical mo-cap systems
Sensors	Image sensor
Pros	Accurate in translation measurement
Cons	Difficult to setup, indoor
System type	Depth sensing camera or scanner
Sensors	An infrared projector combined with a monochrome CMOS sensor
Pros	Skeleton trajectory, facial detection and gesture sensing can all be achieved
Cons	Limited vision range, indoor
System type	Inertial sensors mo-cap system
Sensors	(i). Inertial measurement unit (IMU)
	(ii). IMU and electromyography (EMG) sensor
	(iii). IMU and Magnetometer
Pros	(i). Easy to setup
	(ii). Good gesture sensing ability
	(iii). Accurate in orientation computation
Cons	Gyroscope data drifts over time and accurate translation computation is hard to achieve with 100Hz or lower sampling rate

gravity on three axes are often referred to as MARG, and have been used for advanced monitoring of aircraft attitudes, including roll, pitch, and yaw [20]. Based on MARG, a quaternion algorithm is developed for the drift compensation that makes it possible to achieve indoor navigation where GPS cannot work [21, 22].

Depth camera based systems have also been used for human motion monitoring. The depth camera measures the points' distance of the captured scene, and its price and data accuracy have become attractive with the invention of Microsoft Kinect. Unlike the Wii MotionPlus console, Kinect monitors the whole human body and it requires players to move the same way instructed by the gaming role. However, depth camera still has occlusion problem, and can only measure from a limited distance.

Researches showed that the human body movements can be estimated with muscle activities using Electromyography (EMG) signal alone or a combination of EMG and IMU to obtain more details [23, 24]. Myo (Thalmic Labs Inc.), which provides 8 EMG pods and a 9-axis IMU in an armband, has many applications in motion sensing. Myo has been used in gesture control experiments. Although it has so many advantages, it requires eight nodes for each hand that makes it impractical for users.

For ADLs monitoring, to track trajectory of one's motions regardless of indoor or outdoor, a portable or wearable device is the best choice. In this paper, we have developed a wearable motion monitoring system using the MARG sensors to track the trajectory of the limbs' motions. A graphic

user interface (GUI) is created in LabVIEW (National Instruments) to collect and process data, and display in real-time. Stored data were analyzed using a quaternion-based motion reconstruction algorithm.

2. System overview

2.1. System architecture

Wireless sensor tags are products that combine sensors with wireless communication to achieve low power wireless sensing function. Based on the wireless communication technology, there are four common types of wireless sensor tags in the market; RFID such as MLX90129, by Melexis [25], Wi-Fi such as Wireless Sensor Tag Pro, by Cao Gadgets [26], ZigBee such as Z302E Wireless asset tag, by Netvox technology CO [27], and Bluetooth low energy (BLE) such as Texas Instrument's CC2541 SensorTag [28]. MLX90129 doesn't have motion sensors and it is bulky; hence, not suitable for monitoring human motions. Both MLX90129 and Wireless Sensor Tag Pro are used for temperature or humidity monitoring. The power consumption of Wi-Fi is higher compared to BLE and ZigBee. Finally, ZigBee is not supported by most of the smartphones while BLE is.

CC2541 SensorTag is developed to furnish Internet of Things (IoT) designs [29], and it is the first development kit using BLE. CC2541 SensorTag has six sensors including infra-red (IR) temperature sensor, humidity sensor, pressure sensor, accelerometer, gyroscope, and magnetometer. At full operation, the SensorTag continuously runs on a 230 mAh coin cell battery (i.e., CR2032). It is small enough to be worn, as the length and width of the board are 5.6 cm and 2.5 cm, respectively. The SensorTag development kit, a USB dongle that connects to computer, and a customized wristband are shown in figure 1.

The block diagram of the SensorTag is shown in figure 2. Each SensorTag is composed of a CC2541 that is a system-on-chip (SoC) module comprising an 8051 microcontroller (MCU), a wireless transceiver (BLE), and a 12-bit analog to digital converter (ADC). The MCU not only controls the BLE module and ADC, but also manages external components (six sensors, a side key, LEDs, etc.). In addition, CC2541 provides 23 general purpose I/O lines, six timers (one 16-bit, two 8-bit, one BLE link layer timer, one watchdog timer for reset, and one sleep timer), two universal synchronous /asynchronous receiver/transmitter (USART) ports, and one I²C bus. Because all the sensors are equipped with internal ADCs, the information from the sensors is read by the MCU through the I²C bus [30].

The SensorTag firmware is programmed in the IAR embedded workbench (IAR Systems). The firmware first initializes the hardware, then enables the interrupts, runs power on self-test, and at last it starts Operating System Abstraction Layer (OSAL). OSAL provides scheduling, memory management and message features for the SensorTag. There are 11 events in the OSAL scheduling, the first ten events are executed to enable the BLE, and the eleventh one is

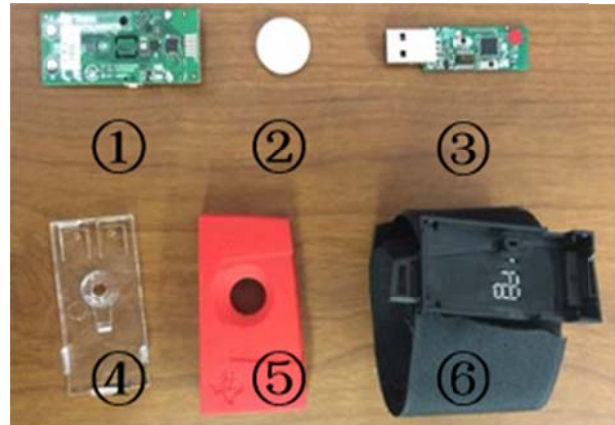


Figure 1. Number ① to ⑥ show different components of a CC2541 SensorTag, which includes the main tag, coin cell battery (CR2032), CC2540 USB dongle, plastic cover, enclosure, and cover sewn on the Velcro strap, respectively.

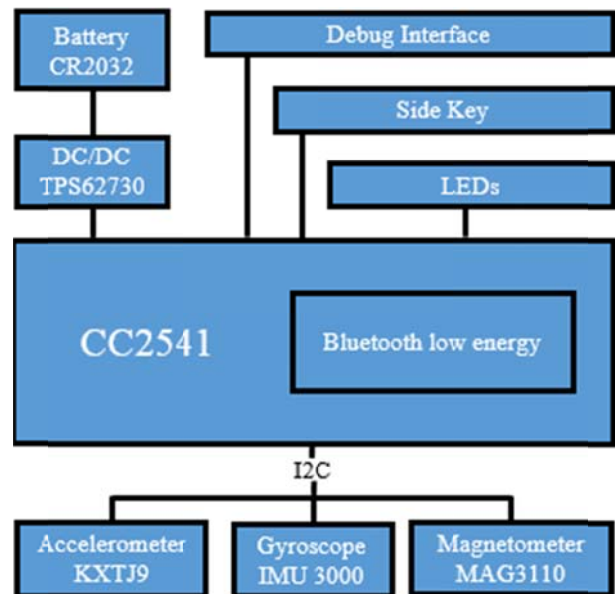


Figure 2. CC2541 Bluetooth low energy SensorTag block diagram is shown. There are six sensors controlled by the CC2541, however, the developed system only utilizes the accelerometer, gyroscope and magnetometer.

called the SensorTag event, which handles the system reset function (press the side key), initializes the sensors, turns on the BLE advertisement and waits for the connection request from the dongle. The firmware flowchart is shown in figure 3. After the power is turned on, the SensorTag initializes the board and executes the OSAL events to start advertisement. It keeps advertising until receives the connection request from the dongle, and then the sensors are enabled to send data. The firmware provides a sampling rate of 50 Hz for the tri-axial MARG sensors. When the SensorTag receives the termination commands from the dongle, it stops reading

from the sensors and returns to advertisement status. By turning off the power, the SensorTag stops advertising.

We have adopted 6 SensorTags, developed firmware, and a GUI to simultaneously acquire signals from the MARG sensors available on the SensorTags. The 6 sensor tags can be used to cover the whole body or body parts, to create a wireless body area network (WBAN) for motion monitoring. For each tag, a CC2540 USB dongles is needed on the base station side to receive data and send information to GUI for displaying and further processing. The system topology in the context of communicating with a smartphone, where only one sensor tag can be active at a time, and communicating with the base station, where all 6 sensor tags can operate simultaneously, is shown in figure 4. It's possible to connect two or more SensorTags to the smartphone at the same time as the master device can connect to multiple (maximum 7) slave devices, although the application used in this paper can only have access to one SensorTag at a time.

2.2. Graphic user interface

GUI is developed in LabVIEW. The program runs in a flat sequence structure; it first sets the COM port number, baud rate and buffer size, and then sends two commands to initial-

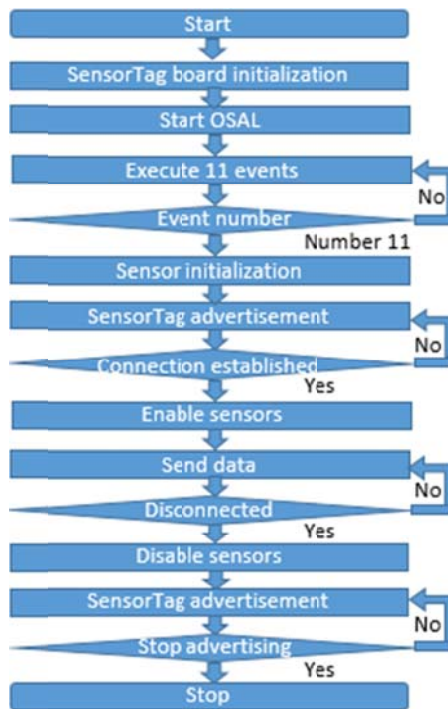


Figure 3. The firmware flowchart is shown. The firmware first initializes the hardware, then enables the interrupts and runs power on self-test, at last it starts Operating System Abstraction Layer (OSAL). OSAL executes multiple events including scheduling, memory management and message features, and finally the eleventh which is the SensorTag event. SensorTag event initializes the sensors, and waits for commands to perform read and write.

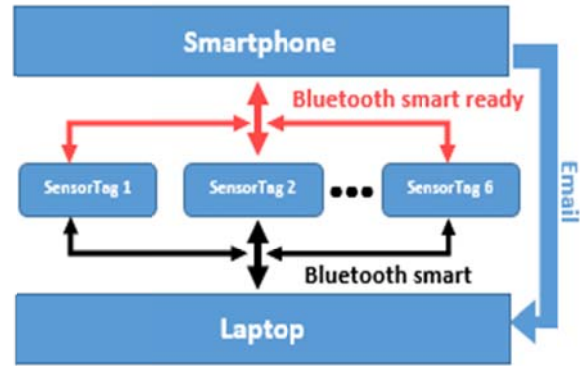


Figure 4. System topology is shown. Six SensorTags are tested to work simultaneously with a stationary unit (a laptop and 6 BLE dongles connected to it) via Bluetooth. The smartphone (Bluetooth smart ready) can connect to the SensorTag and send data in “CSV” format through email to the user. Although the SensorTag iOS application of Texas Instruments can only connect to one SensorTag, it is possible to develop a customized application to connect to all six SensorTags.

ize the dongle. After that, it will scan for 10 seconds. If the SensorTag is advertising, a link would be established, and a sensor initialization command would be sent out to the SensorTag. The SensorTag follows the flowchart shown in Fig. 3, and the GUI would receive the signals within 5 seconds. Finally, when the user presses the stop button, the received data and timestamp would be stored in the stationary PC, and the SensorTag would go back to advertising status. The flowchart of the GUI is shown in figure 5. The front-panel of the GUI developed in LabVIEW is shown in figure 6.

2.3. Motion reconstruction using a quaternion-based algorithm

There are three main types of orientation estimation algorithms (OEAs). The first OEA benefits from Kalman filter or extended Kalman filter (EKF), which uses the current measured signals to predict the certainty of future signals. This OEA uses Kalman gain as a weighted average to achieve the efficient optimized tilt calculation. The problem with Kalman-based OEA is that the frequently updated gain increases the computational burden [31, 32].

Mahony et al. (2008) proposed an OEA based on a complementary filter, which applies a low-pass filter to accelerometer signals and a high-pass filter to gyroscope signals to compute the tilt angle [33]. This algorithm has a system error in computing the angle when the rotation angle approaches to $\pm\pi$ radian [32].

Madgwick et al. (2011) introduced a computationally inexpensive quaternion-based OEA that is suitable for tri-axial MARG sensors when the sampling rate is low (e.g. 10Hz) [34]. Due to efficiency, this OEA can be a practical substitute, especially when the parameters of the algorithm have been adjusted carefully according to the ADLs monitoring results [35, 36].

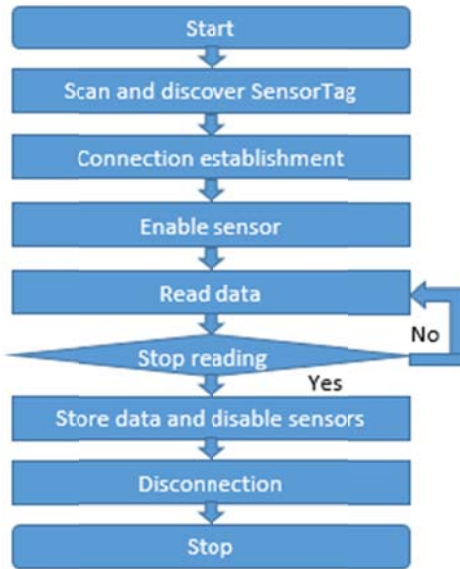


Figure 5. The LabVIEW program flowchart is shown. The program first reads the COM ports and start scanning for the SensorTags. After the link is established, it receives configuration information, and enables the sensors. Then the program displays the signals in real-time. When the “Stop” button is pressed, data would be saved and disconnect from the SensorTags.

Gyroscope measures the angular rate for orientation; however it drifts over time and needs the directions of gravity (accelerometer) and earth magnetic field (magnetometer) as references for revision. The accelerometer measures acceleration in three axes, where the z axis comprises a baseline due to the gravity (g -force = 9.81 m/s^2 straight upwards), and it can be used to fix the tilting errors in X and Y

axes. The magnetometer measurement is not affected in Z axis as its direction is not vertical unless in geomagnetic poles. In this paper, the MARG sensors’ data is used to obtain quaternion and rotation matrix to achieve the revision.

Quaternion system is used to represent the orientation including three types of deflection angles; roll (ϕ), pitch (θ) and yaw (ψ). If the position changes from sensor (S) frame to earth (E) frame, then ${}^E_S\hat{q}$ can be used to represent the change in the matrix shown in equation (1), where α is the frame deflection angle shown in figure 7, r_x , r_y , and r_z are MARG sensors’ data in this context. It is assumed that $\alpha_0 = 0$ to obtain equation (2) when the position changes from sensor frame to earth frame. MARG sensors’ quaternions are obtained with more complex computation like cross product and integration using ${}^E_S\hat{q}$, MARG sensor vectors (sensor frame) shown from equation (3) to (5), S_ω , S_a , and S_m , represent information obtained from gyroscope, accelerometer, and magnetometer, respectively. Unit vectors in earth frame for accelerometer and magnetometer are shown in equations (6) and (7), E_a and E_m , respectively.

$${}^E_S\hat{q} = [q_1 \ q_2 \ q_3 \ q_4] = \begin{bmatrix} \cos \frac{\alpha}{2} & -r_x \sin \frac{\alpha}{2} & -r_y \sin \frac{\alpha}{2} & -r_z \sin \frac{\alpha}{2} \end{bmatrix} \quad (1)$$

$${}^E_S\hat{q} = [1 \ 0 \ 0 \ 0] \quad (2)$$

$$S_\omega = [0 \ \omega_x \ \omega_y \ \omega_z] \quad (3)$$

$$S_a = [0 \ a_x \ a_y \ a_z] \quad (4)$$

$$S_m = [0 \ m_x \ m_y \ m_z] \quad (5)$$

$$E_a = [0 \ 0 \ 0 \ 1] \quad (6)$$

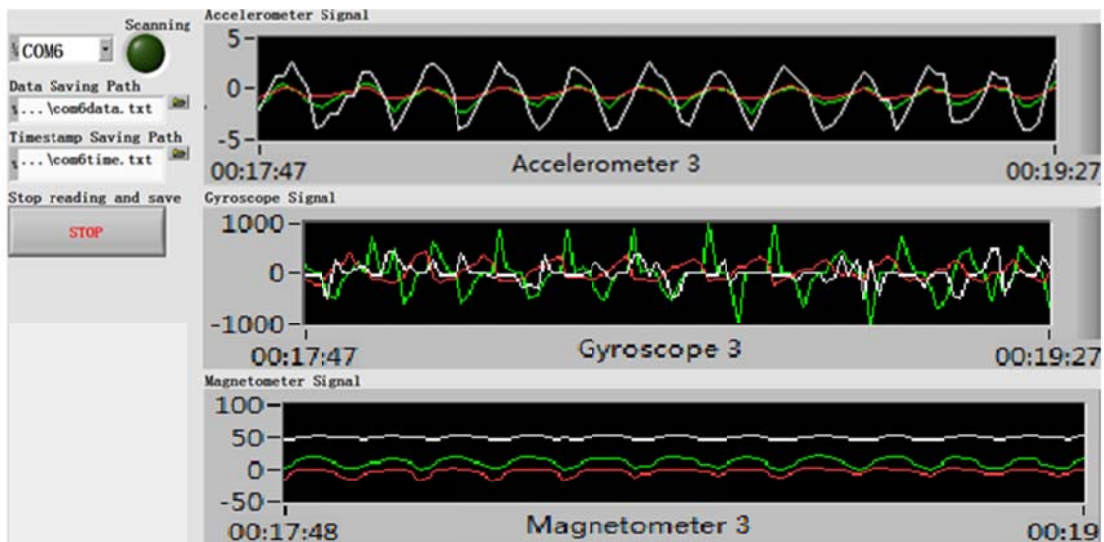


Figure 6. The front panel of the SensorTag graphical user interface is shown. User should select the COM port(s) first, and then run the program. If the wireless link is established between the tag(s) and the base station, the signals would be displayed.

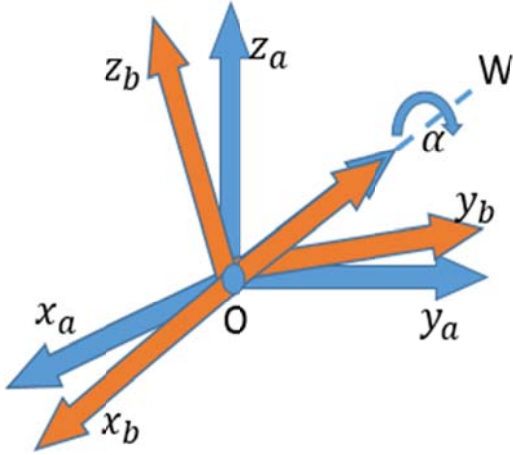


Figure 7. Position “A” changes to position “B”, and “W” axis rotates an angle of “ α ”.

$$E_m = [0 \quad \sqrt{x^2 + y^2} \quad 0 \quad z] \quad (7)$$

Five quaternions, based on equations (3) to (7) are used to calculate rotation matrices ($g_s^E R$, $a_s^E R$, $m_s^E R$, $a_{unit}^E R$ and $m_{unit}^E R$) following equation (8). The $g_s^E R$ has inherent drift problems due to gyroscope technology. By comparing $a_s^E R$ and $a_{unit}^E R$, the errors in X and Y axes can be obtained. By comparing $m_s^E R$ and $m_{unit}^E R$, the errors in Z axis can be obtained. The errors can be used to revise the $g_s^E R$ to get a more reliable rotation matrix ($^E R$) for the deflection angles calculation following equations (9) to (11). The whole process from quaternion generation to obtaining deflection angles is shown in figure 8.

$$^E R = \begin{bmatrix} 2q_1^2 - 1 + 2q_2^2 & 2(q_2q_3 + q_1q_4) & 2(q_2q_4 - q_1q_3) \\ 2(q_2q_3 - q_1q_4) & 2q_1^2 - 1 + 2q_3^2 & 2(q_3q_4 + q_1q_2) \\ 2(q_2q_4 + q_1q_3) & 2(q_3q_4 - q_1q_2) & 2q_1^2 - 1 + 2q_4^2 \end{bmatrix}$$

$$= \begin{bmatrix} \cos \psi \cos \theta & \cos \psi \sin \theta \sin \phi - \sin \psi \cos \phi & \cos \psi \sin \theta \cos \phi - \sin \psi \sin \phi \\ \sin \psi \cos \theta & \sin \psi \sin \theta \sin \phi + \cos \psi \cos \phi & \sin \psi \sin \theta \cos \phi - \cos \psi \sin \phi \\ -\sin \theta & \cos \theta \sin \phi & \cos \theta \cos \phi \end{bmatrix} \quad (8)$$

$$\psi = \text{atan2}(2(q_2q_4 + q_1q_3), 2q_1^2 - 1 + 2q_2^2) \quad (9)$$

$$\theta = -\sin^{-1} 2(q_2q_4 + q_1q_3) \quad (10)$$

$$\phi = \text{atan2}(2(q_3q_4 - q_1q_2), 2q_1^2 - 1 + 2q_4^2) \quad (11)$$

$$a = \sqrt{a_x^2 + a_y^2 + a_z^2} \quad (12)$$

Acceleration calculation is shown in equation (12).

The velocity changes every t seconds, and velocity and distance can be obtained, assuming the initial velocity is 0:

$$v_t = v_{t-1} + a_{t-1} \times t \quad (13)$$

$$s_t = s_{t-1} + v_{t-1} \times t \quad (14)$$

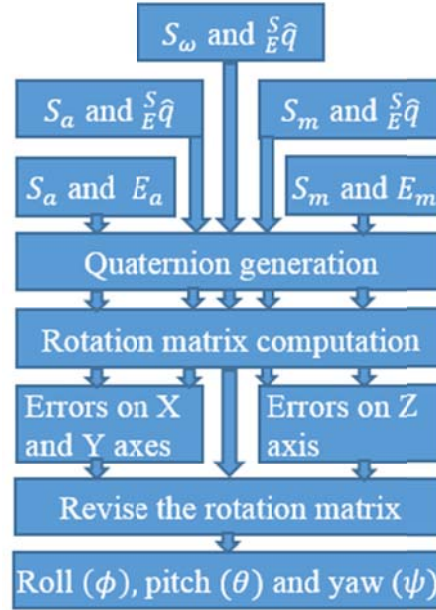


Figure 8. The process from quaternion generation to deflection angles obtainment is shown.

3. Functional and measurement results

The system was validated in three different scenarios: 1) linear displacement, 2) eating gesture, and 3) walking on a straight path. The results for each test are represented in the following.

3.1. Monitoring linear displacement

For this experiment, an optical marker was attached to a SensorTag, and the SensorTag was moved by the experimenter on a linear path along a 60-cm ruler, inside a motion capture lab. The data from the SensorTag and motion capture systems were recorded simultaneously, and stored for off-line comparison. Figure 9, shows the trajectories from the two systems. The camera trajectory is almost straight with 5.18 cm error, while the SensorTag's curved at about 24.74 cm that caused an error of 9.58 cm. This is due to the lack of orientation revision in the Y axis. As a result, the linear displacement of the SensorTag and camera systems from the start to end points was calculated as 55.2 cm and 58.81 cm, respectively, assuming the distance is equal to $\sqrt{x^2 + y^2 + z^2}$. The error rates (ϵ) that are computed from equation (15), yield 7.99% error for the SensorTag system, and 1.99% for the camera system.

$$\epsilon = \frac{|Total \ true \ distance - Total \ calculated \ distance|}{Total \ true \ distance} \times 100\% \quad (15)$$

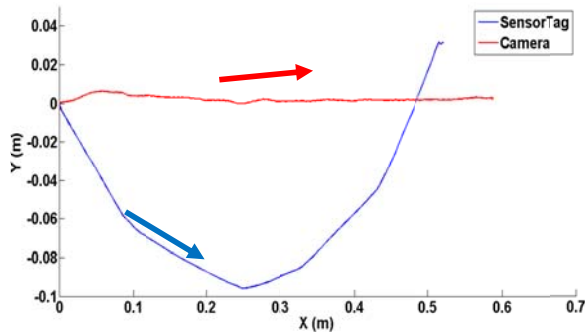


Figure 9. Two trajectories based on SensorTag and camera are shown. The trajectory of camera system is almost a straight line, and most of it stayed in X-Y phase. SensorTag system’s trajectory started around (0, 0, 0), and ended at (0.5213, 0.0312, -0.1787). Both systems demonstrated a distance travel around 60 cm, however, the SensorTag OEA didn’t result into a straight trajectory.

3.2. Monitoring food intake gesture

To monitor subjects’ upper limb motions, ‘food intake experiments’ were conducted, where a subject sat on a chair wearing one SensorTag on the wrist, pretended to “grasp” food from a table in front of him, and took food into the mouth. When finished the subject put his hand back to the armrest of the chair. The experiment was repeated for 20 times for each hand. An example for the food intake trajectory is shown in figure 10. The figure should represent a closed-loop trajectory as the subject start the task from the armrest, and finishes in the same place. There are two turning points, the first one is after the “grasping” gesture (labelled as ①), and the second one is after the “intaking” gesture (labelled as ②). The distance between the starting and ending points was calculated as 23.13cm. Five trials of the same gesture, which are plotted in figure 11, showed the food intake pattern is repeatable. The statistical results from

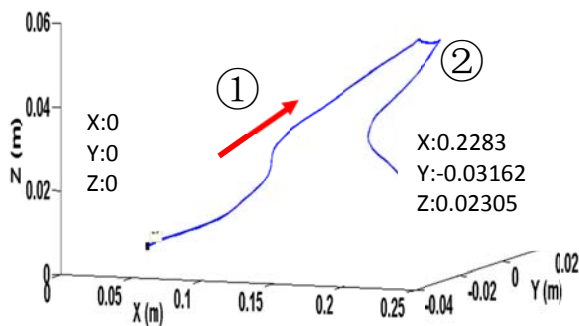


Figure 10. Eating gesture monitoring trajectory plot is shown. The distance between the starting point and the ending point is around 23.13 cm. Turning point ① is after the “grasping” gesture, and turning point ② is after the “food in-taking” gesture.

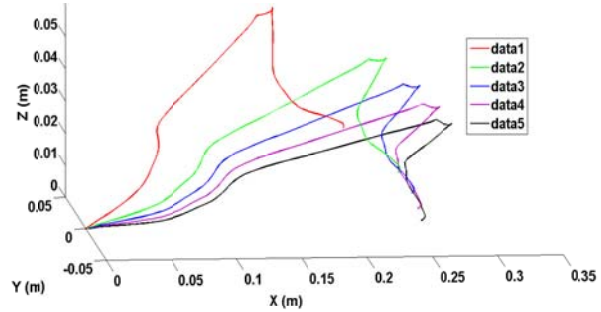


Figure 11. Food intake pattern of five trials is shown. The “grasping” and “food in-taking” gestures are distinctive.

40 tests are shown in table 2, as mean \pm standard deviation (STD). The gyroscope has a higher error in Z axis compared to X and Y axes, which is due to the drift in the Z-axis caused by the inherent limitation in the technology used to build the gyroscopes. This drift is even present in the high-end gyroscopes used in aviation industry.

Table 2. Eating gesture monitoring resulted from 40 trials on each hand.

Right hand	Mean \pm STD (cm)
Distance	33.74 \pm 6.53
X-axis error	15.07 \pm 10.90
Y -axis error	14.29 \pm 9.91
Z -axis error	28.75 \pm 7.73
Left hand	
Distance	35.52 \pm 5.92
X-axis error	17.20 \pm 8.12
Y -axis error	16.24 \pm 6.61
Z -axis error	30.05 \pm 7.10

3.3. Monitoring walking on straight path

In this test, a subject wore six SensorTags, one on the wrist, knee, and ankle joints, of the left and right sides. The subject was asked to walk on a straight path that was 3.96 meters (13ft) for 10 times. An example of the reconstructed trajectories of all six joints is shown in figures 12 to 14.

The reconstructed trajectories in figure 12 showed the end (x, y, z) values as (0.5446, 0.1143, 0.0463) and (0.8717, 0.0169, 0.0526), for the right and left wrists, respectively. The end values for the right and left ankles were calculated as (4.4550, -0.0011, 0.2872) and (3.7010, 0.2626, 0.0777), respectively (figure 13). The trajectory in figure 14 showed that end points for right and left knee joints were (3.0500, 0.1766, 0.0356) and (2.1810, 0.1113, 0.0802), respectively.

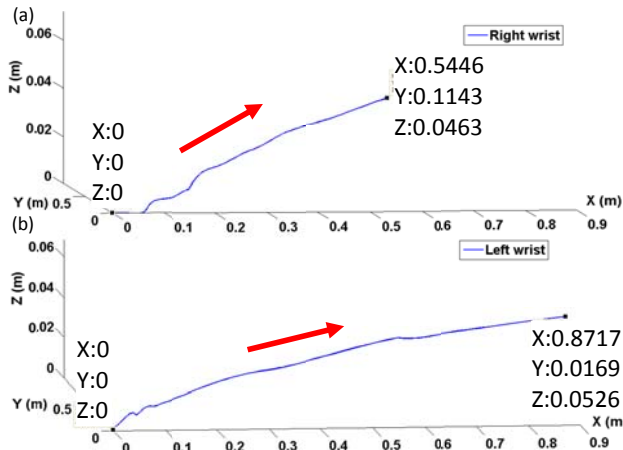


Figure 12. Wrist joints' trajectories are shown. The short distance is due to the fact that the wrist and knee joints do not necessarily travel as long as the ankle joints.

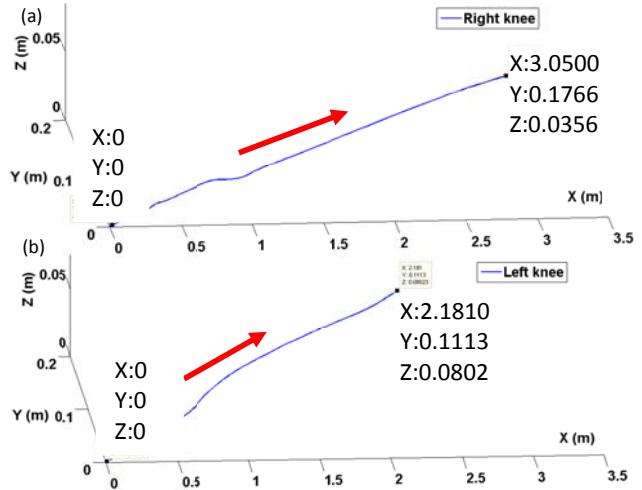


Figure 14. Knee joints' trajectories are shown. The distance is longer than the wrists', but shorter than the ankles'.

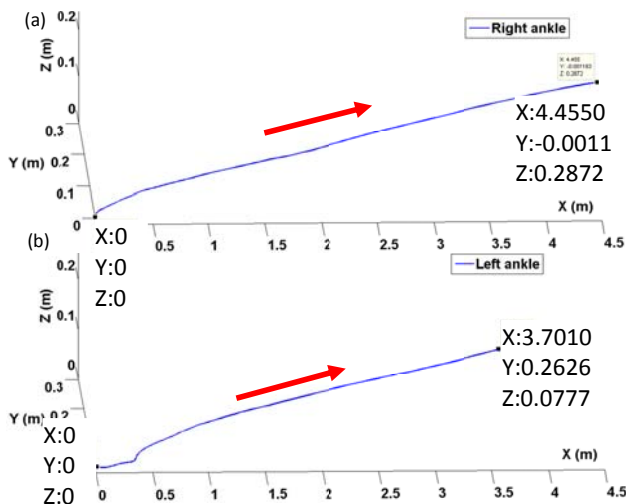


Figure 13. Ankle joints' trajectories are shown. Ankle moved straighter and longer than the wrists and knees. The reason that the ankle joint does not reflect the travelled distance is due to the gyroscope drift that was discussed above.

The reason that the wrist and knee joints moved less than the ankle joints is partially due to the fact that the wrist and knee joints do not necessarily travel as long as the ankle joints. The reason that the ankle joint does not reflect the travelled distance is due to the gyroscope drift that was discussed above.

The total displacement of each joint is shown in Table 3. The error rates of SensorTag translation on the right and left ankles are computed using equation (15), yield 7.07% for the right ankle and 12.67% for the left ankle. The statistical results from the 10 tests are shown in table 4.

Table 3. The total displacement of the wrist, knee and ankle joints.

Left or right	Joint name	
	Left	Right
Wrist	0.8734 m	0.5583 m
Knee	2.1849 m	3.0555 m
Ankle	3.6822 m	4.4645 m

Table 4. Walking monitoring results on both ankles.

Right ankle	Mean ± STD
Distance (m)	3.82 ± 1.14
X-axis error (cm)	21.19 ± 5.30
Y -axis error (cm)	26.96 ± 7.12
Z -axis error (cm)	28.29 ± 6.48
Left ankle	
Distance (m)	3.78 ± 0.92
X-axis error (cm)	22.56 ± 6.33
Y -axis error (cm)	26.74 ± 5.72
Z -axis error (cm)	29.41 ± 6.90

4. Conclusion and future work

In this paper, we have developed a wireless wearable motion monitoring system that is suitable for monitoring ADLs involving limbs. The system is inexpensive, and utilizes commercially-available MARG sensors for real-time motion

data collection. The accuracy of the system was tested in different scenarios, and compared to a camera-based mo-cap system or a measurable criterion.

Linear displacement tests demonstrated our system is less accurate than the camera-based mo-cap systems; however, the error rate is still under 8%. While the proposed system is much cheaper than the camera-based mo-cap systems, it is also easier to set it up, especially in the outdoor scenarios. This is valuable to monitor activity of subjects while they are not limited to indoor.

For the food in-take test, we mimicked the process and reconstructed the food in-take motion pattern. The error in X and Y axes of 40 tests on each hand are in acceptable range (less than 20 cm), while the Z axis error reached 30 cm due to the use of low quality gyroscope.

In the walking test, hands moved back and forth, and the OEA calculates the relative acceleration, which leads to a different result from the knee and ankle movements. The knee and ankle joints' movements are almost in a straight line, hence, the motion reconstruction results are more reliable and the error rates of ankle joints in these tests are less than 13%.

Based on the results, there are three ways to improve the system in the future. First, utilize a better gyroscope in the SensorTag to avoid drifting problem. Second, develop a customized OEA for the ADLs' monitoring that has improved orientation and displacement calculation. Finally, a more practical smartphone application could be developed to connect six or more SensorTags simultaneously, and save data in higher sampling rates.

References

- [1] WHO (World Health Organization), (2001). International Classification of Functioning, Disability and Health (ICF). WHO (World Health Organization), Geneva.
- [2] Katz, S., et al. (1963) Studies of Illness in the Aged; The Index of ADL: A Standardized Measure of Biological and Psychosocial Function. *JAMA*. 185(12):914-919
- [3] Lawton, M.P., & Brody, E.M. (1969). Assessment of older people: Self-maintaining and instrumental activities of daily living. *The Gerontologist*, 9(3), 179-186.
- [4] Anderson C.K., et al., (2004). Ability to perform activities of daily living is the main factor affecting quality of life in patients with dementia. *Health Qual Life Outcomes*, 2:52.
- [5] Qing, Z., et al. (2014). Activity of Daily Living assessment through wireless sensor data. *Engineering in Medicine and Biology Society (EMBC)*, 2014 36th Annual International Conference of the IEEE.
- [6] Qing, Z., et al. (2013). Determination of Activities of Daily Living of independent living older people using environmentally placed sensors. *Engineering in Medicine and Biology Society (EMBC)*, 2013 35th Annual International Conference of the IEEE.
- [7] World Population Ageing. (n.d.). Retrieved August 30, 2016, from <http://www.un.org/esa/population/publications/worldageing19502050/>
- [8] Hindle, J. V. (2010). Ageing, neurodegeneration and Parkinson's disease. *Age and Ageing* 39(2): 156-161.
- [9] Yuting, Z., et al. (2011). Continuous functional activity monitoring based on wearable tri-axial accelerometer and gyroscope. *Pervasive Computing Technologies for Healthcare (PervasiveHealth)*, 2011 5th International Conference on.
- [10] Rui, W., et al. (2014). Automatic identification of solid-phase medication intake using wireless wearable accelerometers. *Engineering in Medicine and Biology Society (EMBC)*, 2014 36th Annual International Conference of the IEEE.
- [11] Palmerini, L., et al. (2011). Dimensionality reduction for the quantitative evaluation of a smartphone-based Timed Up and Go test. *Engineering in Medicine and Biology Society, EMBC*, 2011 Annual International Conference of the IEEE.
- [12] Johansson, G. (1973). "Visual perception of biological motion and a model for its analysis." *Perception & Psychophysics* 14(2).
- [13] Hoflinger, F., et al. (2013). "A Wireless Micro Inertial Measurement Unit (IMU)." *Instrumentation and Measurement, IEEE Transactions on* 62(9): 2583-2595.
- [14] Che Ujang, B., et al. (2011). "Quaternion-Valued Nonlinear Adaptive Filtering." *Neural Networks, IEEE Transactions on* 22(8): 1193-1206.
- [15] Jahanchahi, C., et al. (2012). On gradient calculation in quaternion adaptive filtering. *Acoustics, Speech and Signal Processing (ICASSP)*, 2012 IEEE International Conference on.
- [16] Byung-Seop, K., et al. (2013). IMU-WPS hybrid position estimation test-bed development. *Industrial Engineering and Engineering Management (IEEM)*, 2013 IEEE International Conference on.
- [17] Dongpo, X. and D. P. Mandic (2015). "The Theory of Quaternion Matrix Derivatives." *Signal Processing, IEEE Transactions on* 63(6): 1543-1556.
- [18] Hata, R. and K. Murase (2014). Quaternion neuro-fuzzy for real-valued classification problems. *Soft Computing and Intelligent Systems (SCIS)*, 2014 Joint 7th International Conference on and Advanced Intelligent Systems (ISIS), 15th International Symposium on.
- [19] Jahanchahi, C. and D. P. Mandic (2014). "A Class of Quaternion Kalman Filters." *Neural Networks and Learning Systems, IEEE Transactions on* 25(3): 533-544.
- [20] Madgwick, S. O. H., et al. (2011). Estimation of IMU and MARG orientation using a gradient descent algorithm. *Rehabilitation Robotics (ICORR)*, 2011 IEEE International Conference on.
- [21] Lanlan, L., et al. (2015). "Quaternion Approach to the Measurement of the Local Birefringence Distribution in Optical Fibers." *Photonics Journal, IEEE* 7(4): 1-14.
- [22] Gait trajectorying with x-IMU | x-io Technologies. (n.d.). Retrieved August 30, 2016, from <http://x-io.co.uk/gait-tracking-with-x-imu/>
- [23] Wheeler, K. R. (2003). Device control using gestures sensed from EMG. *Soft Computing in Industrial Applications*, 2003. SMCia/03. Proceedings of the 2003 IEEE International Workshop on.
- [24] Xiang, C., et al. (2007). Hand Gesture Recognition Research Based on Surface EMG Sensors and 2D-accelerometers. *Wearable Computers*, 2007 11th IEEE International Symposium on.
- [25] Khojasteh, H., et al. (2012). A two-tier integrated RFID/sensor network with a WiFi WLAN. *Wireless Communications and Mobile Computing Conference (IWCMC)*, 2012 8th International.
- [26] Minh-Son, N. and L.-T. Quan (2014). Low-power and cost-effective wifi sensor motes for wireless embedded Internet applications. *Advanced Technologies for Communications (ATC)*, 2014 International Conference on.

- [27] Chau-Chung, S., et al. (2011). Simulation and experimental analysis of a ZigBee sensor network with fault detection and reconfiguration mechanism. Control Conference (ASCC), 2011 8th Asian.
- [28] Allen, B., et al. (2013). Evaluation of fall risk for post-stroke patients using bluetooth low-energy wireless sensor. Global Communications Conference (GLOBECOM), 2013 IEEE.
- [29] Duk-jin, K., et al. (2012). Fault detection and isolation in motion monitoring system. Engineering in Medicine and Biology Society (EMBC), 2012 Annual International Conference of the IEEE.
- [30] Teardown of a Bluetooth Low Energy (BLE) device. Retrieved August 30, 2016, from <http://teelengineering.com/tear-down-of-a-bluetooth-low-energy-ble-product/>
- [31] Choukroun, D., et al. (2012). Quaternion Estimation from Vector Observations using a Matrix Kalman Filter. Aerospace and Electronic Systems, IEEE Transactions on 48(4): 3133-3158.
- [32] Jahanchahi, C. and D. P. Mandic (2014). A Class of Quaternion Kalman Filters. Neural Networks and Learning Systems, IEEE Transactions on 25(3): 533-544.
- [33] Mahony, R., et al., (2008). Nonlinear complementary filters on the special orthogonal group. IEEE Trans. on Automatic Control, 53, 1203– 1218.
- [34] Madgwick, S., et al. (2011). Estimation of imu and marg orientation using a gradient descent algorithm. In IEEE Int. Conf. on Rehabilitation Robotics (ICORR), 1–7.
- [35] A. Cavallo, et al. (2014). Experimental comparison of sensor fusion algorithms for attitude estimation. Proc. IEEE IFAC, pp.7585 -7591
- [36] Vaccarella, A., et al. (2013). Unscented Kalman Filter Based Sensor Fusion for Robust Optical and Electromagnetic Tracking in Surgical Navigation. Instrumentation and Measurement, IEEE Transactions on 62(7): 2067-2081.